Performance of slurry photocatalytic membrane reactor for the treatment of real secondary wastewater effluent polluted by anti-cancer drugs

Raphael Janssens*[a], Robin Hainaut[a], Juline Gillard[a], Helene Dailly[b], Patricia Luis[a]

[a]Materials Process Engineering (iMMC-IMAP), Universite catholique de Louvain, Place Sainte Barbe 2, 1348 Louvain-la-Neuve, Belgium

[b]Earth and life institute (ELI), Universite catholique de Louvain, Place Croix du Sud 2, 1348 Louvain-la-Neuve, Belgium

*corresponding author: raphael.janssens@uclouvain.be

Highlights

- Catalyst cake layer does not improve membrane separation performances
- After 150 hours of operation, membrane separation performances were stable
- Catalyst aggregation in real wastewater did not influence membrane fouling
- Wastewater ionic content permeating through reverse osmosis hinders photocatalysis

Abstract

The emergence of non-biodegradable and persistent compounds in European surface waters calls for the development of innovative advanced water treatments. Therefore, this work aimed to assess the performance of a slurry photocatalytic membrane reactor to treat secondary wastewater effluent polluted by anti-cancer drugs. Results show that the 100 kDa Al_2O_3 membrane effectively rejected TiO_2 catalyst particles. Furthermore, stable water permeabilities and separation properties were observed during 150 hours in secondary wastewater at optimized operating conditions. However, significant deterioration of photocatalytic degradation rates were obtained in real effluent when compared to laboratory grade water experiments. An innovative matrix filtration methodology developed in this study permitted to conclude that the negative effects of real effluent were principally imputed to ions present in real matrix. This study concluded that photocatalytic membrane reactor is a promising technology for advanced water treatment, but still requires the development of catalyst to operate on real effluents.

1 Introduction

Recent occurrence studies have correlated the amount of anti-cancer drugs detected in European surface waters to the amount administrated to patients [1, 2, 3, 4, 5]. Several pharmaceuticals have properties which can explain this pollution: limited metabolization by the human body, high urine excretion ratio [1], and low-biodegradability [6]. Therefore, drugs studied in this work were selected based on these properties: 5-fluorouracil, capecitabine, and cyclophosphamide. After being administrated to patients, a fraction of the parent drug is thus excreted and carried away together with its metabolites through sewage systems towards municipal wastewater treatment plants where biological digestion and disinfection steps are conducted. However, the oxidizing power of the currently applied municipal wastewater treatment plant is insufficient to fully degrade such stable pharmaceutical compounds. Related environmental issues are complex to assess because anti-cancer drugs, metabolites, and oxidized by-products were shown to be toxic [7, 8]. An additional aspect calling for the development of appropriate water treatment is the dynamic of the world population histogram: the number of people aged 60 or over is expected to rise worldwide in the coming decades (962 million in 2017, 1.4 billion in 2030, and 2.4 billion in 2050) [9], and the main risk factor for cancer development is advancing age [10].

The present work investigates the potential of slurry photocatalytic membrane reactor (PMR) for degrading anti-cancer drugs spiked in real secondary wastewater effluent. Several published studies report efficient removal rates of anti-cancer drugs by UV/TiO_2 processes which transform energy conveyed by photons into free oxidative radicals [11, 12, 13, 14, 15, 7, 16]. Literature indicates that complex water matrices such as wastewaters hinder oxidizing power of photocatalytic systems due to catalyst active site deactivation and/or radical scavenger effect assigned to ionic species and natural organic mater [17, 18, 19, 20, 21, 22]. Additive methodologies are generally applied to investigate the effects of one or several species in a pure matrix possibly missing complex interaction occurring in real samples. Therefore an innovative sub-

tractive method was developed and applied in this work to identify species most responsible for photocatalytic deactivation using sequential batch filtration steps (nanofiltration and reverse osmosis).

In comparison to immobilized catalyst systems, the suspension of particles in slurry PMRs, investigated in this work, allows to increase the catalyst surface area exposed to UV. However, the slurry feature requires a filtration module to confine catalyst particles in the PMR system. Because polymeric membrane showed low resistance to UVs and free oxidative radicals, as well as abrasion induced by repetitive catalyst-membrane contact [23, 24], ceramic membrane are preferentially selected for PMR applications [25]. Another advantage of the ceramic membranes stands in the possibility to recycle the ceramic material, as published by several studies [26, 27]. This advantage was shown to reduced investment costs while producing eco-friendly membranes [28]. A stability study performed by Mozia et al. on three ceramic TiO_2 membranes of different pore sizes (5kDa and 100 kDa ultrafiltration and $0.2\mu m$ microfiltration) showed that the membrane with the most stable separation properties and permeate fluxes was the 100kDa ultrafiltration membrane (100 h operation). Furthermore, at low cross-flow velocity (CFV) values, deposition of catalyst particles was observed on membrane surface [29] leading to the formation of a cake layer which increased the overall filtration resistance. Another study on the same membrane observed a reduction of separation properties after 400 hours of filtration at a higher CFV of 6 m/s [30]. These works highlight that ceramic membranes are subject to abrasive effects but to a lower extent than polymeric ones. The present study investigates further the cake layer formation mechanisms in real wastewater matrices and their impact on separation properties. To the knowledge of the authors, this study evidences important information related to the behavior of slurry PMR systems operating on real wastewater effluents.

2 Material and methods

2.1 Materials and handling precautions

Three anti-cancer drugs were purchased from Sigma-Aldrich at the highest purity grade available ($> 98\,\%$): 5-fluorouracil, capecitabine, and cyclophosphamide. Molecular structures are presented in Figure 1. Stock solutions (1 mg/mL) of these toxic drugs were prepared in MilliQ water following safety guidelines [31]. Samples and stock solutions were stored in the dark at -20°C as recommended in a stability study by Negreira et al. [32]. Also, the molecular probe - para-chlorobenzoic acid (pCBA) - described by Elovitz and Von Gunten was used to measure indirectly the presence of free hydroxyl radical in solution [33]. The highest purity grade available for this compound was purchased from Sigma-Aldrich, Germany and the TiO_2 photocatalyst (P25, $70/30 - wt\,\%$ anatase/rutile) was purchased from Evonik Degussa, Germany.

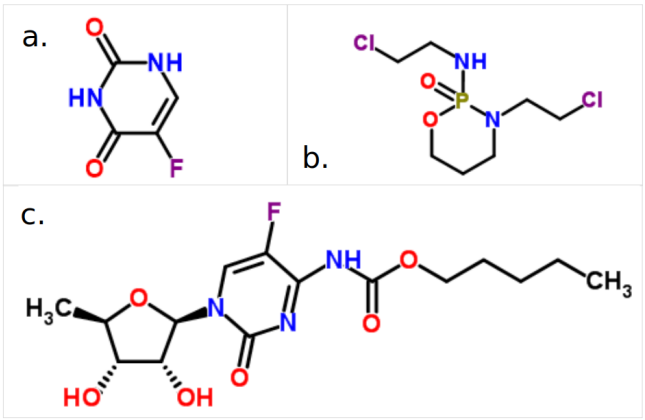

Figure 1: Molecular structure of (a) 5-fluorouracil, (b) cyclophosphamide and (c) capecitabine drawn on *www.chemSpider.com*

2.2 Water characterization

Two water matrices were investigated: the laboratory grade water (LGW) produced by a MilliQ water system (Millipore, CA, USA; Resistivity:18.2 $M\Omega$ at 25°C; $TOC < 5\mu g.L^{-1}$;

bacteria $< 1\,CFU.mL^{-1}$; particulates $< 0.22\mu m$) and secondary wastewater effluent collected at the outlet of the last treatment step of a municipal wastewater treatment plant located in Louvain-la-Neuve, Belgium. Single grab samples were collected in March 2019, stored in the dark at $4°C$, and used for experiments within 10 days. Biological oxygen demand (BOD), total suspended solids (TSS), total nitrogen, nitrogen, and total phosphorous content of water samples were analyzed by the treatment plant operator. The other characteristics presented in Table 1 were analyzed in our laboratories: pH (WTW - inoLab pH meter, Germany), chemical oxygen demand (COD) with the Spectroquant COD cell kit (4 - 40 mg/L) while sulfate, nitrate, phosphate, chloride, bicarbonate and calcium content were measured by ion-exchange chromatography using the Ion Chromatography System Dionex ICS-2000.

2.3 Sequential batch filtration method

To identify which water species were impacting most photocatalytic performances, the secondary wastewater effluent was filtered consecutively through a nanofiltration (YMSESP3001 from Steriltech at a TMP of 15 bars) and a reverse osmosis (YMDLSP3001 from Steriltech at a TMP of 25 bars) flat sheet membrane using an Armfield FT17 cross-flow filtration system. Volumes permeated were collected and stored in dark conditions at $4°C$ for further photocatalysis essays with pCBA. Characteristic of the secondary wastewater effluent (WWeff), NF-permeate and RO-permeate are presented in Table 1. In addition, rejection values (R) were calculated for each membrane based on the concentration of each species (i) in the wastewater effluent ($C_{WWeff,i}$) and in the permeate ($C_{permeate,i}$) using the Equation 1.

$$R_i = \frac{C_{WWeff,i} - C_{permeate,i}}{C_{WWeff,i}} \tag{1}$$

2.4 Photocatalytic membrane reactor

Anti-cancer drugs have been detected in European hospital wastewaters at levels of 124 $\mu g/L$ for 5-fluorouracil [34] and at 100 $\mu g/L$ for carboplatin [35]. Therefore, the same order of magnitude of concentrations were selected for oxidation experiments by spiking individually 5-fluorouracil, cyclophosphamide, and capecitabine at 500 $\mu g/L$ in the studied water matrix. This concentration was selected as low as possible taking into account the limits of detection (10 $\mu g/L$) of the analytical method (UPLC-MS).

Table 1: Characteristic of the secondary wastewater effluent (WWeff) permeated through nanofiltration (NF-permeate) and reverse osmosis (RO-permeate) membranes, and corresponding rejection values (R), ionic content, biological oxygen demand (BOD), total suspended solids (TSS), and chemical oxygen demand (COD).

	WWeff	NF-permeate		RO-permeate	
	mg/L	mg/L	R	mg/L	R
(a) BOD	0.5	-	-	-	-
(a) TSS	0	-	-	-	-
(a) Tot. N	5.42	-	-	-	-
(a) Tot. P	3.2	-	-	-	-
(b) COD	8.1	<4	-	<4	-
(b) SO_4^{2-}	63.4	34	46%	10.6	83%
(b) NO_3^-	2.1	1.6	24%	0.4	81%
(b) PO_4^{3-}	2.6	1.8	31%	n.d.	>90%
(b) Cl^-	444	227	49%	93	79%
(b) HCO_3^-	265	-	-	55	79%
(b) Ca^{2+}	101	-	-	12	88%
(b) pH	7.1	7.1	-	7.1	-

(a) analysed by treatment plant operator
(b) analysed in our laboratories
(n.d.) non detected
(-) not analysed

2.4.1 Experimental setup

The photocatalytic membrane reactor was composed of a double-jacket photocatalytic reactor and a cross-flow filtration module, as presented in Figure 2. One low-pressure mercury lamp

(10W, Elios Italquartz, Italy) was immersed in the 1.3 L reactor which was thermoregulated at 20°C by a cooling system (Microcool MC250, Lauda, Germany). The low-pressure mercury lamp had a monochromatic emission spectrum at 254 nm (supplier data). Furthermore, a double diaphragm pump (XPX1, Wilden, UK) was used to circulate and pressurize the aqueous solution at 3 bars in the lumen side of a 100 kDa tubular ceramic membrane purchased from Atech Innovation, Germany. The photocatalytic reactor was connected to a membrane module in order to confine the suspended catalyst in the system allowing for continuous treatment. The selected membrane has an active separation layer made of ZrO_2 and supported on a tubular support made of Al_2O_3. The active surface area is 4.7 $10^{-3}\,m^2$, and the external/internal hydraulic diameter equals 10mm/6mm.

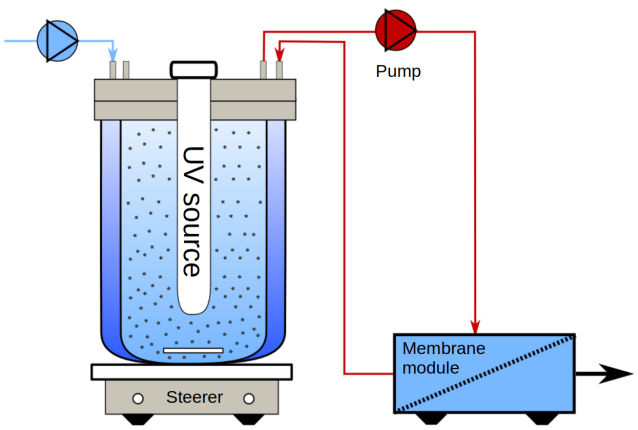

Figure 2: Scheme of the photocatalytic membrane reactor with suspended photocatalytic particles (black stars), the membrane module

2.4.2 Experimental procedures

Feed solutions were prepared by spiking compounds of interest in 1.6 L of the selected water matrix together with the TiO_2 catalyst at a concentration of 1.5 g/L. Then the pump was started in a low flow regime and the feed solution was poured into the reactor. This low flow regime was maintained for 10 minutes to remove eventual air trapped in the system. Afterward, operating conditions were set and the lamps were switched on after a 20 min dark absorption period. At regular intervals (2, 4, 8, 15, 30, 45, and 60 min) 1 mL samples were withdrawn from the reactor

with a syringe and filtered through a cellulose acetate filter which showed low drug absorption rates [36]. This filtration step was performed to avoid any injection of solid matter in the UPLC-MS separation column. Filtered samples were stored at $4°C$ in dark conditions waiting for UPLC-MS analysis. In parallel to each experiment, 100 mL of feed solution were stirred in dark conditions evidencing that the amount of target compound adsorbed on the catalyst was negligible. Also, all pCBA tests were duplicated to plot the standard error of the means in graphs. However, anti-cancer degradation tests were not duplicated to reduce personnel exposure to toxic compounds. To avoid skin exposure to harmful UV rays and eventual toxic drugs splash during filtration, face masks and laboratory coats (Tyvek 400 Dual) were used. Also, waste and reuse management procedures allowed to reduce the volume of toxic waste produced. Aggregation of catalyst particles was visualized thanks to an optical microscope (Olympus Provis AX70, UK). Homogeneous particle distribution was assessed and verified by scanning various areas of each sample with the optical microscope. The TiO_2 concentration in solution was measured by spectrophotometry (DR/400 UV-vis Hach, Germany) at a wavelength of 390 nm working in adsorption mode.

2.4.3 Ceramic membrane characterization

Permeability values (P) were calculated as the volume of solution (ΔV_p) permeating through the active membrane surface area (A) during a fixed amount of time (Δt) at a certain trans-membrane pressure (TMP):

$$P = \frac{1}{A * TMP} \frac{\Delta V_p}{\Delta t} \left[\frac{L}{m^2.h.bar} \right] \tag{2}$$

The overall resistance (R_{ov}) to the water transfer through the membrane was calculated as the inverse of the permeability (P) multiplied by the water viscosity, μ_w ($bar * h$):

$$R_{ov} = \frac{1}{P * \mu_w} [m^{-1}] \tag{3}$$

In addition, separation properties were assessed by filtering Dextran 150 kDa purchased from Sigma-Aldrich, Germany, through the membrane and by calculating its rejection with Equation 1. After each test, the ceramic membrane was cleaned with the following procedure: 2 hours at 250°C in an oven, 20 min of immersion in an ultrasonic bath, 30 min of immersion in an alkaline bath at 80°C (15 g_{NaOH}/L) and 15 min of immersion in an acidic bath at 50°C (1 mL of 75% aqueous H_3PO_4 /L).

2.5 Analytical methods

Dextran concentrations in samples were quantified by evaporative light scattering detector (ELSD, 1200 series Agilent Technologies) using nitrogen as drying gas at 3.5 Bar and 40°C with a gain of 5.

Concentrations of the molecular probe pCBA in samples were quantified by high-performance liquid chromatography (Agilent HPLC 1200 Series HPLC, Agilent Technology, Germany) connected to a diode array detector recording at 240 nm wavelength. 50 μL of sample were injected in a Sorbax Eclipse XDB-C8 column (4.5 x 150 mm, 3.5μm) carried away by a mixture of 80 % methanol and 20 % 25mM NaH_2PO_4 aqueous solution (pH=2.5) at a flow rate of 0.6 mL/min. The column thermostat was set at 30°C.

Concentration of anti-cancer drugs in samples was quantified by ultra-high-pressure liquid chromatography (UPLC 6100 Serie, Agilent Technology, Germany). 5 μL of sample were injected in an HSS5 column (100 x 2.1 mm, 1.8 μm) at a flow rate of 0.3 mL/min leading to retention times shown in Table 2. The solvent gradient presented in Table 2, was adapted from the work of Negreira et al. [37].

Once eluted compounds were detected by an electrospray ionization mass spectrometer (MS 6150 Serie, Agilent Technology, Germany) equipped with a Chemstation software. The mass to charge ratios of each drug and fragmenter voltage are presented in Table 3. The source had a nozzle voltage of -1250V and a capillary voltage relative to the needle of 200 V in positive

Table 2: Solvent Gradient used for the high performance liquid chromatography (UPLC-MS) analysis.

Time (min)	0	3	9	12.5	15	17.5	20	22	25
Solvent B %	0	0	35	35	50	95	95	0	0

A: 0.1 % formic acid in Milli-Q
B: 0.1 % formic acid in acetonitrile

mode and -1500 in negative mode. The dry gas was high purity nitrogen flowing at 8 mL/min at $250°C$ and the nebulizing gas was delivered at 30 psig.

Table 3: Retention times and mass to charge ratio of the three studied anti-cancer drugs.

	5-fluorouracil (−)	cyclophosphamide (+)	capecitabine (+)
Retention time (min)	1.6	9.9	11
Detection (m/z)	129	261	360
Fragmenter voltage (V)	100	175	100

(−) : negative mode
(+) : positive mode

3 Results and discussion

3.1 Catalyst filtration

To understand the behavior of PMR in secondary wastewater effluent (WWeff), the permeability (P) of the PMR system was first measured with the laboratory grade water (LGW) without catalyst added. At a cross-flow velocity (CFV) of 6 m/s and transmembrane pressure (TMP) of 3 bars, a value of 190 $L/(m^2.h.bar)$ was obtained with the 100 kDa ceramic membrane using Equation 2. As presented in Figure 3, the suspension of 1.5 g/L catalyst in the reactor did not modify water transmembrane fluxes at CFV of 6 and 3 m/s. Therefore, the presence of catalyst did not add a resistance to the water transfer through the membrane. Also, catalyst concentrations measured by spectrophotometry in the bulk reactor observed were lower than the

theoretical 1.5 g/L, probably due to particle deposition on reactor walls and piping. However, the reduction of CFV to 1 m/s, led to a decrease of the suspended catalyst concentration to 0.53 ± 0.34 g/L. As described by Jiang et al, this decrease of catalyst content corresponds to the deposition of catalyst particles on the membrane surface [29]: at this low CFV, the drag force exercised on catalyst particles induced by filtration overcomes the lift forces coming from turbulences leading to the formation of a catalyst cake layer. Consequently, an increase of water permeation resistance was observed in Figure 3, as permeabilities values started to lower. To avoid catalyst cake formation, the design and surface properties of photocatalytic particles could be tuned in future researches.

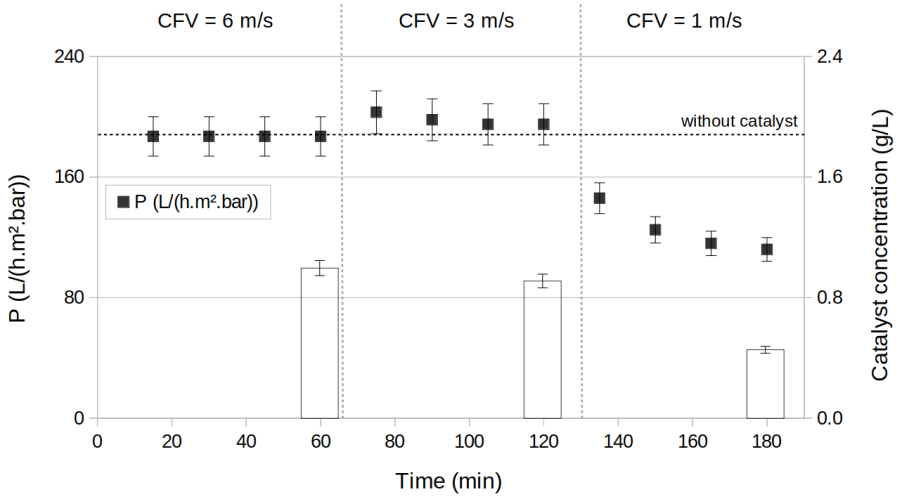

Figure 3: Catalyst concentrations in the reactor and ceramic membrane permeabilities (P) observed without and with 1.5 g/L of TiO_2 catalyst suspended in laboratory grade water (LGW) at different cross flow velocities (CFV) and fixed transmembrane pressure (TMP = 3 bars)

Effects of the real matrix on catalyst filtration was investigated by repeating previous LGW tests on secondary wastewater effluents and reported in Figure 4. Without suspended catalyst, no significant deviation of permeability values were obtained with the two matrices, indicating that organic fouling did not occur (see horizontal dashed lines on Figure 4). The low organic matter content present in the real matrix can explain this observation (see COD value in Table 1).

A similar decrease of permeability was observed in WWeff and LGW effluents when the CFV was

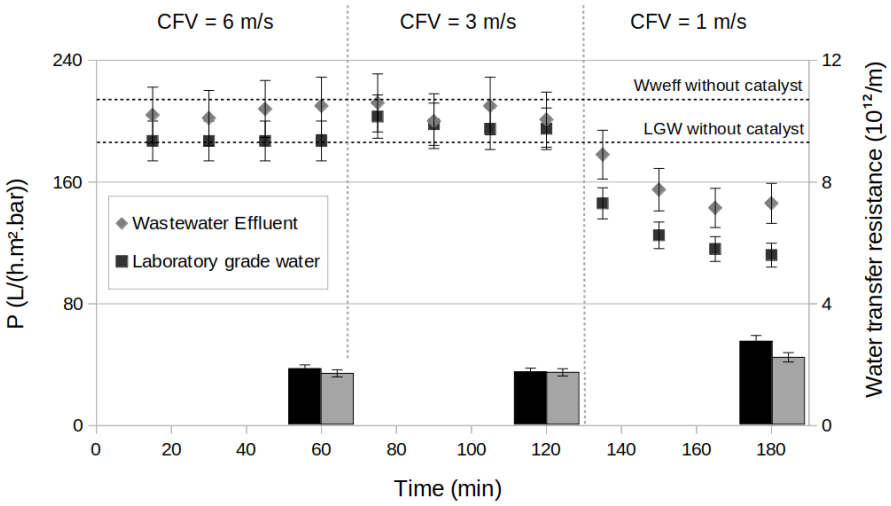

Figure 4: Water transfer resistances and permeabilities (P) through the ceramic membrane observed by filtering 1.5 g/L of TiO_2 catalyst suspended in laboratory grade water and secondary wastewater effluent at different cross flow velocities (CFV) and fixed transmembrane pressure (TMP = 3 bars)

reduced to 1 m/s. However as it can be seen in Figure 4, a more important drop of permeability values was obtained in WWeff ($146 \pm 10\ L/(m^2.h.bar)$) than in LGW ($112 \pm 7\ L/(m^2.h.bar)$). Deviation bars reported in Figure 3 and 4 are standard errors obtained during two different tests performed on two different tubular membranes having the same characteristics. The resistance to water transfer was further analyzed by observing catalyst behavior in the two matrices by optical microscopy. Images indicate that larger clusters of catalyst particles were formed in secondary wastewater effluent (Figure 5b) than in LGW (Figure 5a). TiO_2 particle aggregation is induced by the presence of natural organic matter as well as Ca^{2+} and SO_4^{2-} which modify the photocatalyst surface charge [38]. Therefore, the photocatalyst cake layer formed in WWeff and LGW has different characteristics. The cake layer formed by successive deposition of aggregates of larger size (in WWeff) may induce the development of a cake with higher porosity than the one formed of small aggregates in LGW. The higher porosity is a probable explanation for the lower resistance to water transfer measured in WWeff ($2.74 \pm 0.19 * 10^{12}/m$), when compared to the LGW value ($2.21 \pm 0.15 * 10^{12}/m$).

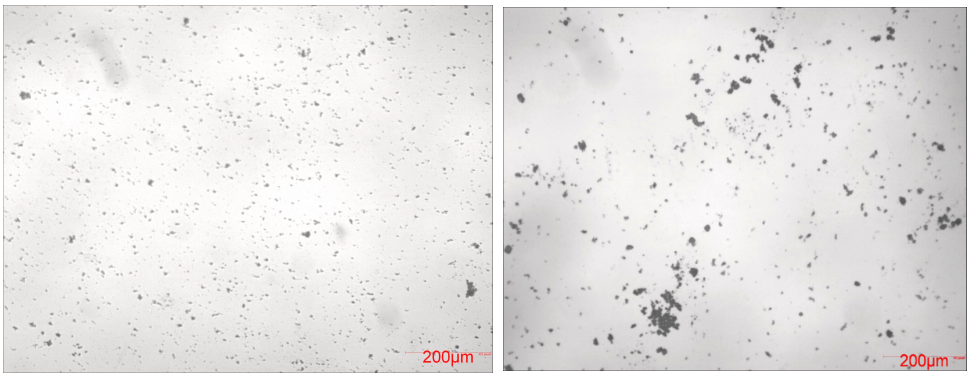

(a) **(b)**

Figure 5: Optical microscope pictures of TiO_2 catalyst (1.5g/L) suspended in (a) laboratory grade water (LGW); (b) secondary wastewater effluent (WWeff)

3.2 Influence of catalytic cake layer on membrane separation properties

The effects of the catalyst cake layer on membrane separation properties were investigated by filtering a compound larger than the 100 kDa membrane molecular weight cut off. Therefore Dextran 150 kDa (1 g/L) was brought into solution with TiO_2 (1.5 g/L) and filtered through the ceramic membrane at a fixed TMP of 3 bars. After 60 min of operation at 3 m/s CFV, the Dextran rejection was measured using equation 1 and then again after 60 min of operation at 1 m/s CFV. Rejection results presented in Figure 6 indicate that the cake layer formed only at CFV of 1 m/s, did not influence Dextran separation. Therefore the exclusion size of the catalyst layer formed in LGW was not smaller than the average membrane pore size of the ceramic membrane.

Another interesting result presented in Figure 6 is the stability of the values obtained for Dextran rejections after 75 and 150 hours of continuous operation at 3 m/s CFV and 3 bars TMP without catalyst cake layer. In addition, stable permeability values were observed during these tests: $P = 187 \pm 7\ L/(m^2.h.bar)$ at $t = 0h$ and $P = 192 \pm 11\ L/(m^2.h.bar)$ at $t = 150h$. Different results were obtained by Szymanski et al. on a 100 kDa membrane made out of TiO_2

(Filtanium, Tami Industries, France), as separation properties decreased after 400 h operation [30]. For future researches, it would be interesting to operate the 100kDa Al_2O_3 membrane, studied in the present work, during 400 h and compare its resistance to abrasion with the one of the Filtanium membrane.

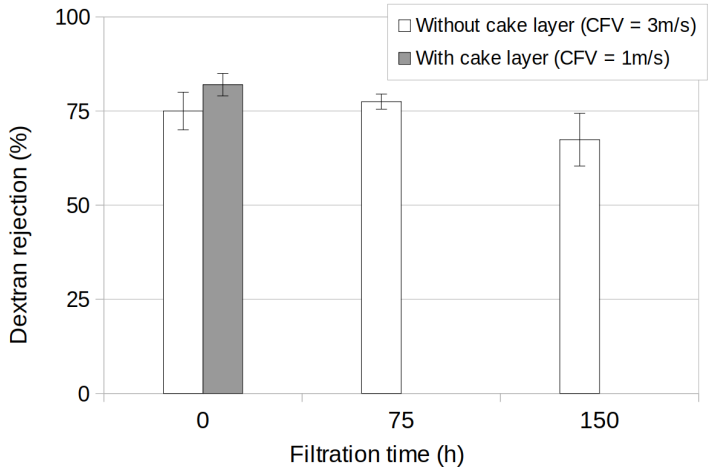

Figure 6: Influence of the catalytic cake layer on the rejection of Dextran 150 kDa by the 100 kDa membrane during 150 hours of continuous filtration in LGW (TMP = 3 bars)

3.3 Catalyst load optimisation

The molecular probe pCBA was used to assess which catalyst concentration led to a maximum production of free hydroxyl radicals by UV/TiO_2 in the photocatalytic membrane reactor. Pseudo-first order kinetics of degradation were observed as pCBA concentration decrease during experiments fitted well the following model: $ln(C/C_0) = -k' * t$ with linear coefficient values above 0.96, with the UV exposure time (t), the pCBA initial concentration ($C_0 = 5\mu M$), and the pCBA concentration during the experiment (C).

To determine the optimal TiO_2 concentration, several catalyst loads were tested and the corresponding pCBA pseudo-first-order apparent rate constants (k') were reported in Figure 7. The non-zero value of pCBA degradation rates ($k' = 0.019\ min^{-1}$) obtained without catalyst in suspension indicates that UV rays can degrade pCBA to a limited extent. Furthermore, the increase of pCBA degradation rates with the addition of catalyst particles up to a load of

1.5 g/L witnesses that free hydroxyl radicals were formed in solution. Above this optimum, penetration lengths of photons in the solution were hindered by the high amount of catalyst particles. This phenomenon referred as light screening in literature [39], was responsible for the decrease of removal rates observed in Figure 7 above 1.5 grams of TiO_2 per litre.

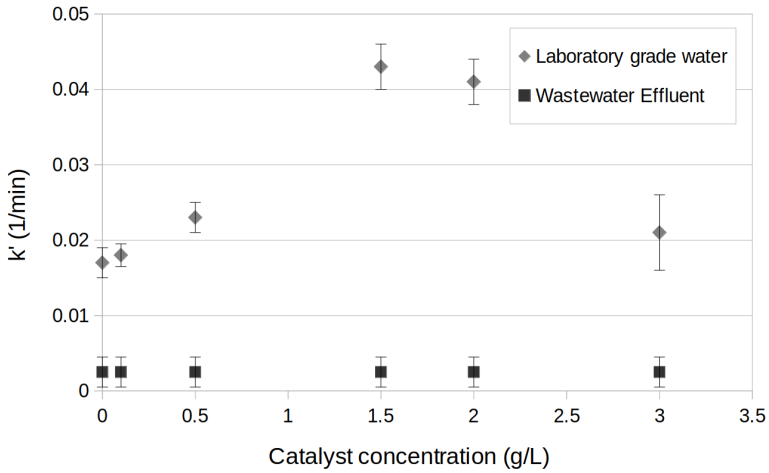

Figure 7: Pseudo-first order apparent rate constants (k') of pCBA degradation in laboratory grade water and secondary wastewater effluent in function of catalyst concentrations

The effect of real water matrix on hydroxyl radical production was investigated by repeating pCBA degradation tests in secondary wastewater effluents. Results presented in Figure 7 show a significant deterioration of apparent degradation rates at every catalyst concentration tested. Before to further investigate and discuss mechanisms inhibiting oxidative radical production (see Sec. 3.5), the influence of secondary wastewater effluents on anti-cancer drugs will be investigated at the optimal catalyst load found in LGW (1.5 g/L).

3.4 Anti-cancer drug degradation

Pseudo-first order apparent rate constants of anti-cancer drugs obtained in LGW and WWeff with and without catalyst added in solution are presented in Figure 8. As it was the case without catalyst for pCBA in LGW, non-negligible degradation rate constants of 5-fluorouracil ($0.042\,min^{-1}$), cyclophosphamide ($0.025\,min^{-1}$) and capecitabine ($0.061\,min^{-1}$) were obtained

in laboratory grade water by direct photolysis. Similar results were obtained for 5-fluorouracil [16], cyclophosphamide [40] and capecitabine [41] in previous publications. An explanation to the higher degradation rate observed for capecitabine can be explained by its higher number of conjugated double bond systems (π bonds) in comparison to 5-fluorouracil and cyclophosphamide molecular structures (see Figure 1). The conjugated double bond can indeed be excited by UV photons and break during relaxation leading to drug degradation.

The addition of TiO_2 catalyst in suspension led to a removal rate increase of the three drugs: 5-fluorouracil (+90%), cyclophosphamide (+250%), and capecitabine (+130%), due to the production of free OH radicals by photocatalytic reactions. This was evidenced by hydroxyl probe tests in section 3.3. Concerning the effects of WWeff on anti-cancer drug degradation, similar negative impacts are observed in Figure 8 as the ones observed in pCBA tests on Figure 7. Chemical species responsible for the deterioration of OH radical production will be discussed in the following section 3.5.

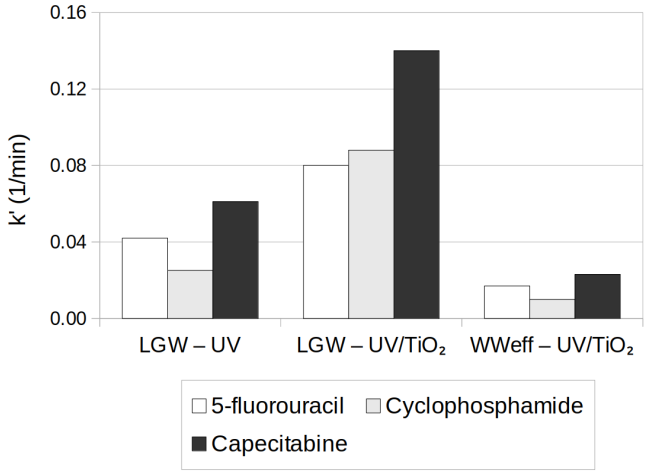

Figure 8: Pseudo-first order apparent rate constants obtained by UV and UV/TiO_2 (1.5 g/L) of three anti-cancer drugs spiked in laboratory grade water (LGW) and secondary wastewater effluent (WWeff) at $500\mu g/L$

3.5 Water matrix influence on photocatalysis

To identify chemical species responsible for photocatalytic deactivation, a sequential batch filtration method was developed and applied on WWeff as described in Section 2.3. pCBA degradation results obtained with 1.5 g/L of catalyst load in laboratory grade water (LGW) and WWeff are reported in Figure 9 together with pCBA degradation results obtained in sequentially filtered WWeff. As it can be seen, rate constants of pCBA degradation in LGW dropped from $0.043 \pm 0.002\, min^{-1}$ to $0.0025 \pm 0.001\, min^{-1}$ in secondary wastewater effluent WWeff. A possible explanation of this inhibition is the presence of natural organic matter present in WWeff (8.1 g/L COD see Table 1). Natural organic matter was shown to deteriorate photocatalytic processes by absorbing UV light and/or scavenging oxidative radicals [42]. However, the pCBA degradation rate remained unchanged when spiked (at $C_0 = 5\mu M$) in the nanofiltered WWeff having a low COD content (see Table 1). Therefore organic matter removal by nanofiltration did not improve the OH radicals formation.

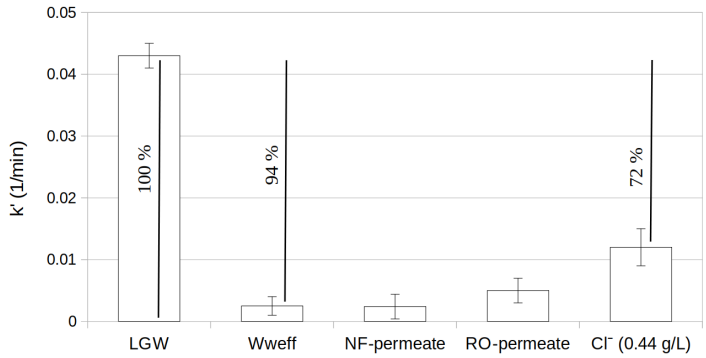

Figure 9: Time-based degradation rate constant of pCBA ($C_0 = 5\mu M$) spiked in different water matrices: laboratory grade water (LGW), secondary wastewater effluent (WWeff), WWeff permeated through nanofiltration and reverse osmosis membrane (NF-permeate and RO-permeate) and Cl^- dissolved in LGW (0.44 g/L)

A sample of the NF-permeate, free of pCBA, was filtered through a reverse osmosis membrane and then observed by optical microscopy. Clusters of catalyst particles were not observed in the RO-permeate sample image, presented in Figure 10, contrarily to the WWeff sample (see Figure 5b). The fact that catalyst aggregation is not observed is probably explained by the removal of

the natural organic matter, Ca^{2+}, and SO_4^{2-} by the RO filtration step known to favor catalyst particle attraction [38]. Furthermore as shown in Figure 9, degradation rates observed in the RO-permeate spiked with pCBA are similar to those observed in the WWeff and NF-permeate matrices. Therefore, the low ionic content of the RO-permeate (see Table 1) is sufficient to deteriorate pCBA degradation. Literature reviews published on this matter indicate that ions can hinder radical formation by different ways [21, 19]: (i) adsorb on catalyst active sites, (ii) scavenge $^{\circ}OH$ to form stable radicals having low oxidizing potentials ($^{\circ}SO_4^-$, $^{\circ}NO_3$, $^{\circ}Cl^-$ or $^{\circ}CO_3^-$) or (iii) modify catalyst surface charge leading to particle aggregation (observed in Figure 5b and 10), and consequently to light screening effects [38, 39]. Furthermore, several studies reported negative impacts of $SO_4^{2-}, NO_3^-, Cl^-, HCO_3^-$ and Ca^{2+} individually dissolved in LGW at higher levels than the ones present in RO-permeate [19, 20]. Therefore, it was concluded from the present results that a real matrix-free of natural organic matter having a low ionic content can significantly hinder OH radical production probably by: site deactivation, radical scavenging, and/or catalyst aggregation.

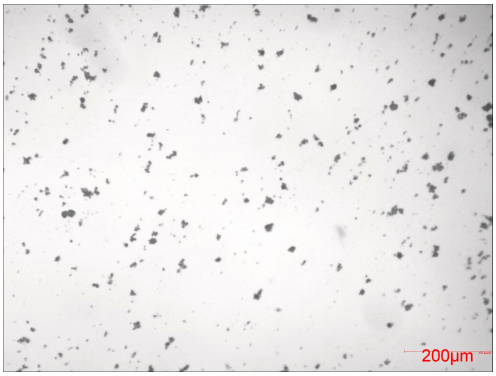

Figure 10: Optical microscope pictures of TiO_2 catalyst (1.5g/L) suspended in reverse osmosis permeate

At last, the effect of the most present ion in WWeff was assessed by dissolving 0.44 grams of Cl^- in 1 liter of LGW. This chloride concentration corresponds to the one measured in WWeff and presented in Table 1. As presented in Figure 9 in comparison to LGW tests (100%), pCBA degradation rates reduction was the highest in WWeff (94%) with a significant impact related to the chloride content present in WWeff samples (72%). The remaining part of the inhibition

observed in WWeff can probably be imputed to the other ions present in RO-permeate HCO_3^-, Ca^{2+} and SO_4^{2-} (see Table 1). To conclude and without taking into account possible synergic ion-ion effects, WWeff chloride content was responsible for a significant reduction of OH radical production in WWeff.

Future researches could aim to develop novel photocatalytic materials being less affected than TiO_2 by real water matrices such as self-organized TiO_2 nanotube arrays synthesized by Ye et al. [22]. However, the strong ionic scavenging effects observed in this work call for the use of alternative oxidation processes such as electrochemical oxidation which turns the presence of chloride into a strength by forming active chlorine species. Finally, future work should assess the toxicity of transformation products formed during advanced oxidation processes. This is a crucial step in the selection of wastewater treatments as transformation products were shown to be more toxic than parent drug compounds [7]

4 Conclusions

The presence of anti-cancer drugs in European surface waters witnesses the fact that currently applied wastewater treatments are not effective to remove certain emerging pollutants. This is attributed to the particular properties of some compounds: limited metabolizations by the human body, high urine excretion ratios, and low-biodegradabilities. As anti-cancer drugs are genotoxic, water treatment plants must be upgraded with novel advanced processes to reduce as much as reasonably possible the pollution of the environment by such chemicals. This work aimed to assess the performance of slurry photocatalytic membrane reactor for treatment of anti-cancer drugs spiked in real secondary wastewater effluent.

To get the required knowledge to operate PMR in secondary wastewater effluent (WWeff), the behavior of the membrane module was investigated first at various operating conditions in laboratory grade water (LGW). Results showed that the investigated 100kDa ceramic membrane made out of Al_20_3 led to effective rejection of TiO_2 photocatalytic particles. At cross-flow velocities (CFV) of 6 and 3 m/s, filtration of the catalytic slurry (1.5 g/L) did not disturb water transfer, however, at 1 m/s a cake layer formed at the membrane surface leading to a reduction of TiO_2 concentration in the reactor and thus to an increase of water transfer resistance through the membrane, from 2.21 ± 0.15 to $2.74 \pm 0.19 * 10^{12}/m$. Also, the presence of the cake layer was shown to have negligible influence on the membrane separation properties as testified by stable Dextran rejection experiments. An important result of this work is that higher permeability values were obtained when the cake layer was formed in wastewater effluent ($146 \pm 10\ L/(m^2.h.bar)$) than in laboratory grade water ($112 \pm 7\ L/(m^2.h.bar)$). The effect of catalyst particle aggregation observed in the real matrix on the cake porosity is a probable explanation for this difference. Furthermore, stable membrane properties were observed during 150 hours of catalyst filtration at 3 m/s CFV in real and pure water matrices. Therefore these operating conditions were used for further degradation tests.

The PMR photocatalytic part aims to produce a sufficient amount of oxidative radicals to de-

grade anti-cancer drugs. Therefore, the TiO_2 concentration leading to the maximum formation of free oxidative radicals was found to be 1.5 g/L in laboratory grade water thanks to degradation tests of a hydroxyl molecular probe. Applying the optimized PMR conditions on pure water matrix spiked with anti-cancer drugs led to significant removal rates of 5-fluorouracil ($0.080\,min^{-1}$), cyclophosphamide ($0.088\,min^{-1}$), and capecitabine ($0.141\,min^{-1}$). However, photocatalytic reactions were inhibited when operating on real wastewater artificially polluted by anti-cancer drugs. An innovative sequential filtration methodology permitted to conclude that the deterioration of hydroxyl formation in the real effluent was related mainly to HCO_3^-, Ca^{2+} and SO_4^{2-} ions with a major contribution of Cl^-. Such ions have the potential to deactivate photocatalytic sites, scavenge OH radicals, and induce catalyst aggregation by modifying particles surface charges. Even though site deactivation could be solved by the future development of photocatalytic materials, ionic scavenging effects call for the use of alternative oxidation processes such as electrochemical oxidation able to turn ions into active oxidizing species.

Acknowledgement

This work was supported by the European Commission through the project ERA-NET Inno Indigo 2014 [Grant number Inn-INDIGO/0002/2014]. The personnel of the Louvain-la-Neuve municipal wastewater treatment plant operated by inBW is gratefully acknowledged for providing wastewater samples.

Abbreviation list

TMP	Transmembrane pressure
CFV	Cross-flow velocity
TMP	Transmembrane pressure
A	Active membrane surface area
V_p	Permeated volume
P	Permeability
μ_w	Water viscosity
R_{ov}	Overall water transfer resistance
pCBA	para-chlorobenzoic acid
LGW	Laboratory grade water
RO	Reverse osmosis
BOD	Biological oxygen demand
COD	Chemical oxygen demand
TSS	Total suspended solid

References

[1] Besse, J. P.; Latour, J. F.; Garric, J. Anticancer drugs in surface waters. What can we say about the occurrence and environmental significance of cytotoxic, cytostatic and endocrine therapy drugs? *Environ. Int.* **2012**, *39*, 73–86.

[2] Booker, V.; Halsall, C.; Llewellyn, N.; Johnson, A.; Williams, R. Prioritising anticancer drugs for environmental monitoring and risk assessment purposes. *Sci. Total Environ.* **2014**, *473-474*, 159–170.

[3] Escudero-Onate, C.; Ferrando-Climent, L.; Rodriguez-Mozaz, S.; Santos, L. *Verlicchi P. (eds) Hospital wastewater*; Hdb Env Chem, Springer, 2017.

[4] Franquet-Griell, H.; Gómez-Canela, C.; Ventura, F.; Lacorte, S. Predicting concentrations of cytostatic drugs in sewage effluents and surface waters of Catalonia (NE Spain). *Environ. Res.* **2015**, *138*, 161–172.

[5] Toolaram, A. P.; Kümmerer, K.; Schneider, M. Environmental risk assessment of anti-cancer drugs and their transformation products: A focus on their genotoxicity characterization-state of knowledge and short comings. *Mut. Res.* **2014**, *760*, 18–35.

[6] Kummerer, K.; Al-ahmad, A.; Bertram, B.; Wieûler, M. Biodegradability of antineoplastic compounds in screening tests : influence of glucosidation and of stereochemistry. *Chemosphere* **2000**, *40*, 767–773.

[7] Lutterbeck, C. A.; Machado, E. L.; Kümmerer, K. Photodegradation of the antineoplastic cyclophosphamide : A comparative study of the efficiencies of UV/H2O2 , UV/Fe2+/H2O2 and UV/TiO2 processes. *Chemosphere* **2015**, *120*, 538–546.

[8] Liu, P.; Zhang, H.; Feng, Y.; Yang, F.; Zhang, J. Removal of trace antibiotics from wastewater: A systematic study of nanofiltration combined with ozone-based advanced oxidation processes. *Chem. Eng. J.* **2014**, *240*, 211–220.

[9] UN, Global issue: ageing. 2018; `https://www.un.org/en/sections/issues-depth/ageing/`.

[10] NCI, Age and cancer risk. 2015; `https://www.cancer.gov/about-cancer/causes-prevention/risk/age`.

[11] Koltsakidou, I.; Antonopoulou, M.; Evgenidou, E.; Konstantinou, I.; Lambropoulou, D. A. Cytarabine degradation by simulated solar assisted photocatalysis using TiO2. *Chem. Eng. J.* **2017**, *316*, 823–831.

[12] Lin, H. H. H.; Lin, A. Y.-C. Photocatalytic oxidation of 5-fluorouracil and cyclophosphamide via UV/TiO2 in an aqueous environment. *Water Res.* **2014**, *48*, 559–568.

[13] Lai, W.; Lin, H.; Lin, A. Y.-C. TiO2 photocatalytic degradation and transformation of oxazaphosphorine drugs in an aqueous environment. *J. Hazard. Mater.* **2015**, *287*, 133–141.

[14] Ofiarska, A.; Pieczyńska, A.; Borzyszkowska, A. F.; Stepnowski, P.; Siedlecka, E. M. Pt-TiO2-assisted photocatalytic degradation of the cytostatic drugs ifosfamide and cyclophosphamide under artificial sunlight. *Chem. Eng. J.* **2016**, *285*, 417–427.

[15] Molinari, R.; Caruso, A.; Argurio, P.; Poerio, T. Degradation of the drugs Gemfibrozil and Tamoxifen in pressurized and de-pressurized membrane photoreactors using suspended polycrystalline TiO2 as catalyst. *J. Membr. Sci.* **2008**, *319*, 54–63.

[16] Zhang, Y.; Xiao, Y.; Zhang, J.; Chang, V.; Lim, T.-T. Degradation of cyclophosphamide and 5-fluorouracil in water using UV and UV/H2O2: Kinetics investigation, pathways and energetic analysis. *J. Environ. Chem. Eng.* **2017**, *5*, 1133–1139.

[17] Chong, M. N.; Jin, B.; Chow, C.; Saint, C. Recent developments in photocatalytic water treatment technology: A review. *Water Res.* **2010**, *44*, 2997–3027.

[18] Habibi, M. H.; Hassanzadeh, A.; Mahdavi, S. The effect of operational parameters on the photocatalytic degradation of three textile azo dyes in aqueous TiO2 suspensions. *J. Photochem. Photobiol. A: Chem.* **2005**, *172*, 89–96.

[19] Lai, W.; Chuang, Y.-C.; Lin, A. Y.-C. The effects and the toxicity increases caused by bicarbonate, chloride, and other water components during the UV/TiO2 degradation of oxazaphosphorine drugs. *Environ. Sci. Pollut. Res.* **2017**, 14595–14604.

[20] Yap, P. S.; Lim, T. T. Effect of aqueous matrix species on synergistic removal of bisphenol-A under solar irradiation using nitrogen-doped TiO2/AC composite. *Appl. Cat. B: Environ.* **2011**, *101*, 709–717.

[21] Rioja, N.; Zorita, S.; Peñas, F. J. Effect of water matrix on photocatalytic degradation and general kinetic modeling. *Appl. Cat. B: Environ.* **2016**, *180*, 330–335.

[22] Ye, Y.; Feng, Y.; Bruning, H.; Yntema, D.; Rijnaarts, H. M. Photocatalytic degradation of metoprolol by TiO2 nanotube arrays and UV-LED: Effects of catalyst properties, operational parameters, commonly present water constituents, and photo-induced reactive species. *Appl. Cat. B: Environ.* **2018**, *220*, 171–181.

[23] Chin, S. S.; Chiang, K.; Fane, A. G. The stability of polymeric membranes in a TiO2 photocatalysis process. *J. Membr. Sci.* **2006**, *275*, 202–211.

[24] Mozia, S.; Darowna, D.; Wróbel, R.; Morawski, A. W. A study on the stability of polyethersulfone ultrafiltration membranes in A photocatalytic membrane reactor. *J. Membr. Sci.* **2015**, *495*, JMS15820.

[25] Janssens, R.; Mandal, M. K.; Dubey, K. K.; Luis, P. Slurry photocatalytic membrane reactor technology for removal of pharmaceutical compounds from wastewater: Towards cytostatic drug elimination. *Sci. Total Environ.* **2017**, *599-600*, 612–626.

[26] Amin, S. K.; Roushdy, M. H.; El-Sherbiny, S. A.; Abdallah, H. A. M.; Abadir, M. F. Preparation of nano-size ceramic membrane from industrial waste. *Inter. J. Appl. Eng. Res.* **2016**, *11*, 7176–7181.

[27] Tolba, G. M. K.; Bastaweesy, A. M.; Ashour, E. A.; Abdelmoez, W.; Khalil, K. A.; Barakat, N. A. M. Effective and highly recyclable ceramic membrane based on amorphous nanosilica for dye removal from the aqueous solutions. *Arab. J. Chem.* **2016**, *9*, 287–296.

[28] REMEB-H2020, Recycled ceramics for low-cost MBR. *Filtr. Sep.* **2019**, *56*, 20–22.

[29] Jiang, H.; Meng, L.; Chen, R.; Jin, W.; Xing, W.; Xu, N. Progress on porous ceramic membrane reactors for heterogeneous catalysis over ultrafine and nano-sized catalysts. *Chin. J. Chem. Eng.* **2013**, *21*, 205–215.

[30] Szymański, K.; Morawski, A.; Mozia, S. Humic acids removal in a photocatalytic membrane reactor with a ceramic UF membrane. *Chem. Eng. J.* **2015**, 1–9.

[31] Eitel, A.; Scherrer, M.; Kummerer, K. Handling cytostatic drugs : A practical guide. **1999**,

[32] Negreira, N.; López de Alda, M.; Barceló, D. Study of the stability of 26 cytostatic drugs and metabolites in wastewater under different conditions. *Sci. Total Environ.* **2014**, *482-483*, 389–398.

[33] Elovitz, M. S.; Von Gunten, U. Hydroxyl radical/ozone ratios during ozonation processes. I. The R(ct) concept. *Ozone: Sci. Eng.* **1999**, *21*, 239–260.

[34] Mahnik, S. N. Fate of 5-fluorouracil , doxorubicin , epirubicin , and daunorubicin in hospital wastewater and their elimination by activated sludge and treatment in a membrane-bioreactor system. *Chemosphere* **2007**, *66*, 30–37.

[35] Lenz, K.; Koellensperger, G.; Hann, S.; Weissenbacher, N.; Mahnik, S. N.; Fuerhacker, M. Fate of cancerostatic platinum compounds in biological wastewater treatment of hospital effluents. *Chemosphere* **2007**, *69*, 1765–1774.

[36] Negreira, N.; Lopez de Alda, M.; Barcelo, D. Cytostatic drugs and metabolites in municipal and hospital wastewaters in Spain: Filtration, occurrence, and environmental risk. *Sci. Total Environ.* **2014**, *497-498*, 68–77.

[37] Negreira, N.; López de Alda, M.; Barceló, D. On-line solid phase extraction-liquid chromatography-tandem mass spectrometry for the determination of 17 cytostatics and metabolites in waste, surface and ground water samples. *J. Chromatogr. A* **2013**, *1280*, 64–74.

[38] Ottofuelling, S.; Von Der Kammer, F.; Hofmann, T. Commercial titanium dioxide nanoparticles in both natural and synthetic water: Comprehensive multidimensional testing and prediction of aggregation behavior. *Environ. Sci. Tech.* **2011**, *45*, 10045–10052.

[39] Umar, M.; Aziz, H. *Photocatalytic Degradation of Organic Pollutants in Water*; Intech, 2012; Chapter 8.

[40] Kim, I.; Yamashita, N.; Tanaka, H. Photodegradation of pharmaceuticals and personal care products during UV and UV/H2O2 treatments. *Chemosphere* **2009**, *77*, 518–525.

[41] Franquet-Griell, H.; Medina, A.; Sans, C.; Lacorte, S. Biological and photochemical degra-

dation of cytostatic drugs under laboratory conditions. *J. Hazard. Mater.* **2017**, *323*, 319–328.

[42] Uyguner-Demirel, C.; Birben, N.; Bekbolet, M. Elucidation of background or- ganic matter matrix effect on photocatalytic treatment of contaminants using TiO2: a review. *Cat. Today* **2017**, *284*, 202–214.

Table of Contents graphic: